Desalination and Water Treatment
www.deswater.com

doi: 10.5004/dwt.2022.28676

269 (2022) 212–220
September

Thickness of adsorbed water film in underground gas reservoir

Aiguo Hu[a,b,*], Kezhi Li[b], Qilin Xu[a], Pei Xiong[b], Lihong Song[a], Fuhu Chen[b], Hao Zhang[c]

[a]*College of Energy, Chengdu University of Technology, Chengdu 610059, China, email: kangzhCUG@163.com (A. Hu)*
[b]*Research Institute of Engineering and Technique, Sinopec Huabei Sub-Company, Zhengzhou 450006, China*
[c]*Australian School of Petroleum, Faculty of Engineering, Computer and Mathematical Sciences, University of Adelaide, Adelaide, SA 5005, Australia*

Received 17 March 2022; Accepted 10 July 2022

ABSTRACT

The bound water is in the form of capillary water and water film in the sand stone of actual gas reservoir underground. According to the Derjaguin–Landau–Verwey–Overbeek (DLVO) theory, the theoretical calculation model of total disjoining pressure and water film thickness is constructed. Combined with the extended Young–Laplace formula, a graphical method for calculating the water film thickness is proposed. The curve of total disjoining pressure and water film thickness is obtained when the actual water salinity and formation temperature and pressure are considered. In actual gas reservoir with high formation water salinity, the electrostatic repulsion is quite small and only the van der Waals force is the main force to keep the water film stable, so the water film thickness in the gas reservoir is small. Comparing the critical pore radius and water film thickness, it shows that the bound water is mainly in the form of capillary water, and the water film thickness is much smaller than the pore radius, which has a limited influence on the percolation of natural gas. The water film thickness is not so important as thought before when evaluating the effective pores in gas reservoir.

Keywords: Gas reservoir; Capillary pressure; Disjoining pressure; Bound water; Thickness of water film

1. Introduction

The pore-throat configuration of the reservoir underground is very complicated. The bound water in the inorganic pores of sand stone in gas reservoir underground is mainly in the form of capillary water and water film, which has a great influence on the gas permeability [1–3]. The traditional view was that the water film is formed by the adsorption on the surface of the rock particles, and the pore can be effective seepage channel only if the throat radius is greater than the water film thickness. Since the pore size is quite small usually, the water film thickness was thought to be quite important when evaluating the effective pores in gas reservoir.

Many scholars research on the disjoining pressure and the water film thickness. Derjaguin and Churaev [4] defines the disjoining pressure as a mechanical stress that applied to the bulk liquid with a certain thickness of the liquid membrane that reaches the equilibrium state, and he proposes that the disjoining pressure is composed of the electrostatic force, van der Waals force and structural force. Gee et al. [5] tests the water film thickness of air, deionized water and quartz surfaces at room temperature with elliptical polarization technique. Nishiyama and Yokoyama [6] researches the relationship between the pore size distribution and the water film thickness, and explained the effect of water film on water-rock reaction. Ward et al. [7] quantitatively determines the effect of pH and ionic strength on the film thickness and its stability.

* Corresponding author.

In this study, a disjoining pressure model is derived considering a combined effect of temperature, pressure, salinity and interfacial tension, which is based on the Derjaguin–Landau–Verwey–Overbeek (DLVO) theory. Moreover, a graphic method of calculating the water film thickness is proposed.

2. Model principle

2.1. Distribution of gas and water in the reservoir

As shown in Fig. 1, the gas generated from kerogen in shale displaces water in neighboring pores. As the pores are water-wet pores, capillary force is the resistance when the gas is driving water. When the capillary force is greater than the pressure difference between gas and water, the gas can effectively displace the original formation water in the pores. The pore radius determines the size of the capillary force, resulting in a very different state of distribution of the aqueous phase as shown in Fig. 2. In smaller pores, the pore is filled with formation water in the form of capillary bound water. In the pore whose radius bigger than certain critical radius r_c, the center of the pore is filled with gas and the formation water covers the pore walls in the form of water film.

The pore network in reservoir is simplified to the capillary bundle model. For the pores at the same depth Z above the free-water level, the bound water is different due to the difference in the radii of the pores as shown in Fig. 3.

At the Z level above the gas–water interface, or free water level, in a water wet sand stone in gas reservoir, there is a corresponding critical pore radius (r_c), which makes the pressure difference between gas phase and water phase equal to the capillary pressure. As shown in Figs. 3 and 4, in the pores with size of the critical radius (r_c), both capillary water and water film exist, which is:

$$p_c = p_g - p_w = \left(\rho_w - \rho_g\right) gZ = \frac{2\sigma_{gw}\cos\theta}{r_c} \tag{1}$$

where Z is the height above the gas–water interface, m; ρ_g is the gas density, kg/m^3; ρ_w is the water density, kg/m^3; r_c is the radius of the critical pore corresponding to the capillary pressure at Z-position; p_g is the gas phase pressure, Pa; p_w is the water phase pressure, Pa; σ_{gw} is the interfacial tension between gas phase and water phase, N/m; θ is wetting contact angle, °.

At the same Z-depth level above the gas/water interface, if the pore radius $r < r_c$, the pore is filled with capillary water as shown in Figs. 3 and 5. Meanwhile, if the pore radius $r > r_c$, the center of the pore is filled with gas, and the pore wall is covered by water film as shown in Figs. 3 and 6.

In the hydrodynamic equilibrium state, at different depths above the gas/water interface, the capillary pressure of pores increases with increasing Z level. The capillary pressure p_c at certain Z level in the formation underground can be determined by following methods:

- If the gradient of gas pressure and water pressure is known, the capillary pressure p_c can be calculated with Eq. (1), which is the pressure difference between gas and water phase at the same depth.
- Alternatively, if the water saturation at Z-position above the gas–water interface of is known, the capillary pressure p_c can be deduced from capillary pressure injection curve.

2.2. Extended Young–Laplace equation

Capillary pressure is defined as the pressure difference between the two-phase interfaces, and the value is equal to the non-wetting phase pressure minus the wetting phase pressure.

$$p_c = p_g - p_w = \prod + 2H\sigma_{gw} \tag{2}$$

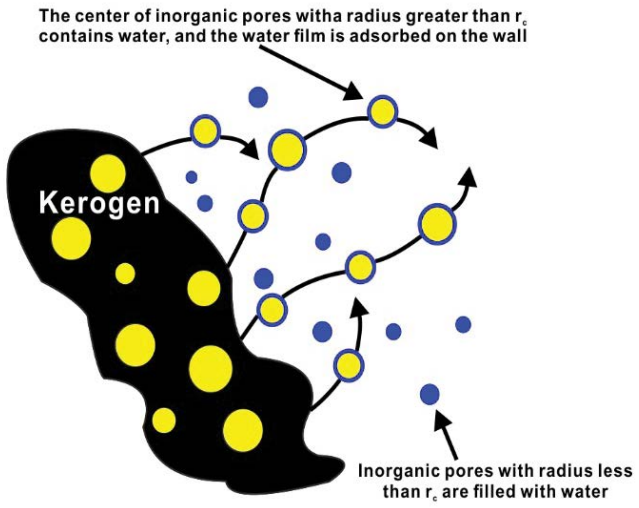

Fig. 1. Displacement of formation water during gas migration.

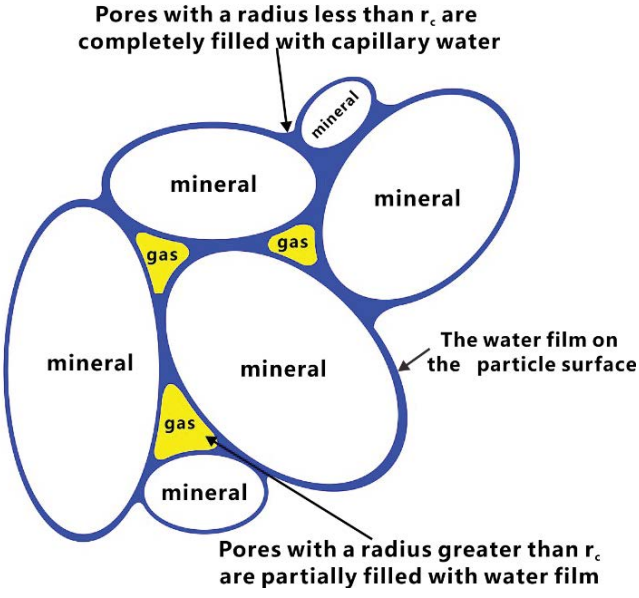

Fig. 2. Distribution of fluids in inorganic pores of sand.

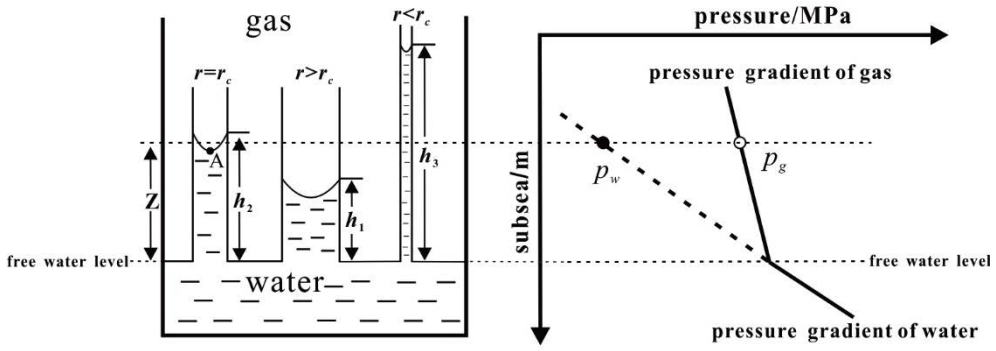

Fig. 3. Relationship between the height of liquid and the capillary pressure in the capillary.

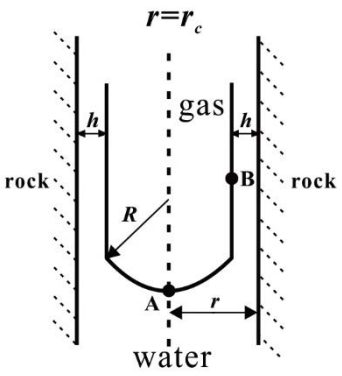

Fig. 4. Distribution of gas and water in the pore ($r = r_c$) at the Z-position above the free water level.

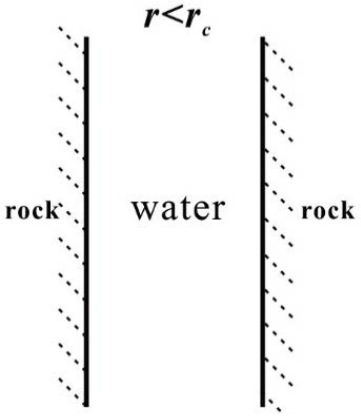

Fig. 5. Distribution of gas and water in the pore ($r < r_c$) at the Z-position above the gas–water interface.

where p_c is capillary pressure, Pa; p_g is gas pressure, Pa; p_w is water pressure, Pa; Π is the rejecting pressure between gas/water interface and water/solid interface of the water film, that is, the disjoining pressure, Pa; H is the mean curvature of solid surface in the water film, 1/m; σ_{gw} is the interfacial tension of gas/water interface, N/m.

The pores network of the reservoir can be reduced to bundle of capillary tubes as shown in Fig. 3. In the capillary tube, Eq. (2) can be rewritten as:

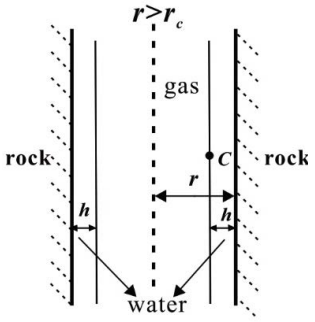

Fig. 6. Distribution of gas and water in the pore ($r > r_c$) at the Z-position above the gas–water interface.

$$p_c = p_g - p_w = \Pi + \left(\frac{1}{R_1} + \frac{1}{R_2}\right)\sigma_{gw} \tag{3}$$

where R_1 and R_2 are the principal radius of curvature of the gas/water interface, respectively, m.

The rock pore system can be characterized by a capillary bundle model. In the hydrophilic capillary, there are two types of microscopic water/gas interface [8], which are discussed separately as following:

2.2.1. Gas/water interface in the capillary tube being of spherical concave shape surface

At the spherical concave surface in the capillary tube shown at point *A* as shown in Figs. 3 and 4, since the water thickness is quite large, so the disjoining pressure Π = 0. Ignoring the thickness changes of water film transition zone at the gas/water/solid three-phase interface, there is:

$$R_1 = R_2 = \frac{r}{\cos\theta} \tag{4}$$

where r is the capillary radius, m and θ is the wet contact angle.

Substituting Eq. (4) into Eq. (3), we get the conventional Laplace formula as:

$$p_c = p_g - p_w = \frac{2\sigma_{gw}\cos\theta}{r} \tag{5}$$

It is noteworthy that, in the capillary pressure injection test of conventional gas reservoir engineering analysis, the capillary pressure is generally expressed with Eq. (5).

2.2.2. Gas/water interface in the capillary tube being of cylindrical shape surface

As shown in Figs. 4 and 6, in the capillary bundle model, the water film is present in the pores in the form of a columnar liquid surface.

Take the point *B* in Fig. 4 or the point *C* in Fig. 6 as an example, since $R_1 = \infty$, $R_2 = r - h$, we can get the following equation from Eq. (3):

$$p_c = p_g - p_w = \Pi + \frac{\sigma_{gw}}{r - h} \tag{6}$$

Hall et al. [9] argued that h can be ignored because the water film thickness is quite small compared to the pore size.

2.3. Disjoining pressure of water film on the pore wall

In the pore with the radius $r \geq r_c$, the relationship between the disjoining pressure of the water film and the capillary pressure is as follows.

2.3.1. In the capillary with the radius $r = r_c$

As shown in Fig. 4, when the radius is $r = r_c$, there is both capillary water and water film in the pore. At the same subsea, there is the following relationships in the hydrodynamic equilibrium state:

$$p_{gA} = p_{gB}, \quad p_{wA} = p_{wB} \tag{7}$$

where p_{gA} is the gas pressure close to *A* point in gas–water interface, Pa; p_{wA} is the water pressure close to *A* point in gas–water interface, Pa; p_{gB} is the gas pressure at *B* point in gas–water interface, Pa; p_{wB} is the water pressure close to *B* point in gas–water interface, Pa.

According to Eq. (5), there is the following relationship at point *A*.

$$p_c = p_{gA} - p_{wA} = \frac{2\sigma_{gw}\cos\theta}{r_c} \tag{8}$$

According to Eq. (6), there is the following relationship at point *B*.

$$p_c = p_{gB} - p_{wB} = \Pi_{eq} + \frac{\sigma_{gw}}{r_c - h} \tag{9}$$

According to Eqs. (6)–(9), the disjoining pressure of the water film is calculated as follows:

$$\Pi_{eq} = p_c - \frac{\sigma_{gw}}{r_c - h} = (\rho_w - \rho_g)gZ - \frac{\sigma_{gw}}{r_c - h} = \frac{2\sigma_{gw}\cos\theta}{r_c} - \frac{\sigma_{gw}}{r_c - h} \tag{10}$$

where h is the water film thickness in the equilibrium condition.

2.3.2. In the capillary with the radius $r > r_c$

As shown in Fig. 6, there is a water film when the pore radius is $r > r_c$. According to Eq. (6), the disjoining pressure of the water film at point *C* is as follows:

$$\Pi_{eq} = p_{gC} - p_{wC} - \frac{\sigma_{gw}}{r - h} = p_c - \frac{\sigma_{gw}}{r - h} \tag{11}$$

where p_{gC} is the gas pressure close to *C* point in gas–water interface, Pa; p_{wC} is the water pressure close to *C* point in gas–water interface, Pa;

Substituting Eq. (1) into Eq. (11) yields the following equation:

$$\Pi_{eq} = p_c - \frac{\sigma_{gw}}{r - h} = (\rho_w - \rho_g)gZ - \frac{\sigma_{gw}}{r - h} \tag{12}$$

Eq. (10) can be seen as a special case of $r = r_c$ in Eq. (12).

2.4. Relationship between disjoining pressure and water film thickness

According to the DLVO theory, the relationship between disjoining pressure and water film thickness can be expressed by the disjoining pressure isotherm. The total disjoining pressure consists of three components:

$$\Pi = \Pi_{DLR} + \Pi_{LVA} + \Pi_S \tag{13}$$

According to Eq. (13), the relationship between the disjoining pressure Π and the water film thickness h at certain temperature and pressure can be calculated. After calculating the disjoining pressure Π_{eq} by Eq. (12), the water film thickness corresponding to the equilibrium disjoining pressure Π_{eq} can be determined graphically in Fig. 7.

How to calculate the three components can be as follows:

2.4.1. Electrostatic forces Π_{DLR}

Assuming the pore wall rock is with negative charge, Gregory [10] proposed the formula of electrostatic forces between parallel plate interfaces to calculate the electrostatic forces between gas/water interface and water/solid interface of the water film on capillary wall:

$$\Pi_{DLR}(h) = n_b k_B T \left\{ \begin{array}{l} 2\left[1 + 0.25\left(\psi_{r1} + \psi_{r2}\right)^2 \csc h^2\left(\frac{\kappa h}{2}\right)\right]^{0.5} \\ -\frac{\left(\psi_{r1} - \psi_{r2}\right)^2 \exp\left(-\kappa h\right)}{1 + 0.25\left(\psi_{r1} + \psi_{r2}\right)^2 \csc h^2\left(\frac{\kappa h}{2}\right)} - 2 \end{array} \right\} \tag{14}$$

$$n_b = N_A \times C, \quad \psi_{ri} = \frac{ze\zeta_i}{k_B T} \tag{15}$$

$$\kappa = \sqrt{\frac{2e^2 z^2 n_b}{\varepsilon_0 \varepsilon_3 k_B T}} \tag{16}$$

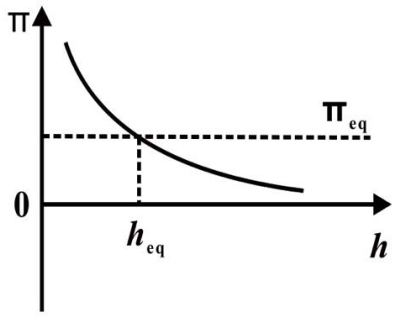

Fig. 7. Graphical determination of water film thickness.

where n_b is the ion concentration (number density) in the bulk solution, 1/m^3; k_B is the Boltzmann constant, the value is 1.38 × 10^{-23} J/K; T is the Kelvin temperature, K; N_A is the Avogadro constant; C is the cationic molarity, mol/m^3; Ψ_{r1} and Ψ_{r2} are dimensionless electrostatic potentials of gas/water interface and water/solid interface, respectively; κ is the reciprocal of Debye length, 1/m; z is cationic valence; h is the water film thickness, m; e is the electronic charge, 1.6 × 10^{-19} C; ζ_i is zeta potential, V; ε_0 is the vacuum permittivity, 8.854 × 10^{-12} F/m; ε_3 is the dielectric constant of water.

In the absence of test data, the dimensionless electrostatic potential of gas/water interface often take 0 [11]. According to the zeta potential ζ_2 of solid minerals in aqueous solution can calculate Ψ_{r2}.

2.4.2. van der Waals force Π_{LVA}

$$\Pi_{\mathrm{LVA}}(h)=\frac{-A\left(15.96\dfrac{h}{\lambda_{\mathrm{lw}}}+2\right)}{12\pi h^3\left(1+5.32\dfrac{h}{\lambda_{\mathrm{lw}}}\right)^2} \tag{17}$$

where h is the water film thickness, m; A is Hamaker constant, J; λ_{lw} is the London wavelength, m.

Gregory [10] recommended London wavelength λ_{lw} = 100 nm with formation conditions. The Hamaker constant is related to the ion type, dielectric constant and temperature in the solid/water/gas three-phase system:

$$A=\left(\sqrt{A_{11}}-\sqrt{A_{33}}\right)\left(\sqrt{A_{22}}-\sqrt{A_{33}}\right) \tag{18}$$

where A_{ii} is the Hamaker constant in a vacuum. And A_{11} for rock minerals; A_{22} for natural gas; and A_{33} for aqueous solutions.

A_{ii} can be calculated with the Lifshitz formula:

$$A_{ii}=\frac{3}{4}k_BT\left(\frac{\varepsilon_i-1}{\varepsilon_i+1}\right)^2+\frac{3f\upsilon_e}{16\sqrt{2}}\frac{(n_i^2-1)^2}{(n_i^2+1)^{3/2}} \tag{19}$$

where the subscript i = 1, 2, 3, representing rock minerals, natural gas and aqueous solutions, respectively; ε is relative dielectric constant; f is Planck constant, 6.62606896 × 10^{-34} J·s; υ_e is the primary electronic absorption frequency in the ultraviolet region, 3 × 10^{15} S^{-1}; n is refractive index.

Tokunaga [11] used the Lifshitz formula to analyze the Hamaker constant of the quartz/brine/CO_2 three-phase system at different temperatures and pressures, and obtain the value in the range of –1.0 × 10^{-20} J to –5.6 × 10^{-21} J. Hall et al. [9] recommends the Hamaker constant of the quartz/saline/gas three-phase system with a value of –3 × 10^{-21} J to –9 × 10^{-21} J. Without considering the lag effect, Chandrasekhar and Rao [12] recommended the Hamaker constant of the quartz/saline/hydrocarbon three-phase system with a value of –1.0 × 10^{-20} J at the ground standard conditions.

2.4.3. Structure forces Π_S

It is produced by the distance between the surfaces of water film and exponential declined with the increase of the water film thickness (h):

$$\Pi_S(h)=\mathrm{A}_s e^{-\frac{h}{h_s}} \tag{20}$$

where A_s is the coefficient, Pa; h_s is the characteristic decay length for the exponential model, m.

Chandrasekhar and Rao [12] recommended A_s with a value of 1.5 × 10^{10} Pa, h_s with a value of 0.05 nm in a quartz/brine/hydrocarbon three-phase system.

The electrostatic force and structural force calculated from Eqs. (14) and (20) are positive. For a quartz/brine/oil three-phase system, because the Hamaker constant is positive, so the van der Waals force calculated from Eq. (17) is negative. For a quartz/brine/gas three-phase system, because the Hamaker constant is negative, Hirasaki [13] took the van der Waals force calculated from Eq. (17) as positive value.

2.5. Calculation method of water film thickness of pore walls in the formation

Sutton proposed to calculate the interfacial tension of gas/water interface with formula as [14]:

$$\sigma_{\mathrm{gw}}=\left[\frac{1.58\times10^{-3}\left(\rho_w-\rho_g\right)+1.76}{T_r^{0.3125}}\right]^4\times10^{-3} \tag{21}$$

Eq. (21) applies only to fresh water. For formation water of high salinity, Eq. (21) should be modified as:

$$\sigma_{\mathrm{gw}}=\left[\frac{1.58\times10^{-3}\left(\rho_w-\rho_g\right)+1.76}{T_r^{0.3125}}\right]^4\times10^{-3}+3.44\times10^{-8}C_s \tag{22}$$

where C_s is salinity, ppm; ρ_g is gas density, kg/m^3; ρ_w is water density, kg/m^3; T_r is reduced temperature, dimensionless variable; σ_{gw} is the interfacial tension between gas and water, N/m.

Eq. (12) is a function of the water film thickness. To calculate the water film thickness in pore with radius r, the following methodology can be employed with iterative procedure in the following steps.

(1) Calculate and draw the curve of total disjoining pressure and water film thickness as given by Eq. (13).

(2) Calculate the capillary pressure p_c with Eq. (1).

(3) Assuming the initial value of water film thickness is $h = h_0$, and calculate the equilibrium disjoining pressure Π_{eq} with the new capillary pressure p_c, interfacial tension σ_{gw} and the supposed pore radius r:

$$\Pi_{eq} = p_c - \frac{\sigma_{gw}}{r - h_0} \tag{23}$$

Get the h_{eq} value corresponding to the disjoining pressure Π_{eq} with graphical method as shown in Fig. 7.

(4) Comparing the difference between h_{eq} and h_0, if it is greater than the allowable error range, make $h_0 = h_{eq}$, and repeat steps (3) and (4), until the difference between h_0 and h_{eq} is negligible.

2.6. Water film thickness in pores at underground condition

Taking a gas reservoir in eastern China as an example, the depth of the reservoir is –2,765 m and the temperature is 130°C (403.15 K). The relative density of the natural gas is 0.56. The aqueous solution is $CaCl_2$ solution and the water at a concentration of 6,000 ppm, or 54 mol/m^3. The relative permittivity of water is 53 F/m, and the wetting contact angle is 35°. According to the mercury injection curve, the measured average pore radius is 611 nm. The interfacial tension of gas/water is 35 mN/m, and the zeta potentials are measured as $\zeta_1 = 0$ mV, $\zeta_2 = -5$ mV.

According to the measured pressure value, the relationship between gas reservoir pressure and altitude is p_g = 22.0255–0.0018334 × H, and the relationship between water pressure and altitude is p_w = 2.19–0.008971 × H. The gas/water interface is assumed to be –2,779 m underground, which is below the bottom of gas pay zone.

2.6.1. Calculation of disjoining pressure

2.6.1.1. Calculation of electrostatic force

With Eq. (16), the calculated Debye κ^{-1} length as follow.

$$\kappa^{-1} = 1/\sqrt{\frac{2\times(1.6\times10^{-19})^2\times2^2\times54\times6.02\times10^{23}}{8.854\times10^{-12}\times53\times1.38\times10^{-23}\times403.15}} = 0.626\text{nm}$$

With Eq. (14), the curve of electrostatic force $\Pi_{DLR}(h)$ vs. water film thickness is shown in Fig. 8.

2.6.1.2. Calculation of van der Waals force

The depth of the middle of the gas reservoir is –2,765 m. The pressure is 27 MPa and the temperature is 130°C. The refractive index and dielectric constant of methane are n = 1.09, ε = 1.13, respectively [15,16]. The refractive index and dielectric constant of water are n = 1.32, ε = 55, respectively. The main rock mineral is quartz and the related parameters shown in Table 1 [17]. With Eq. (19), the Hamaker constant in vacuum is A_{11} = 5.96 × 10^{-20} J, A_{22} = 2.9 × 10^{-21} J, A_{33} = 3.59 × 10^{-20} J. With Eq. (18), the Hamaker constant is –7.42 × 10^{-21} J.

With Eq. (17), the curve of van der Waals force vs. water film thickness is shown in Fig. 9.

2.6.1.3. Calculation of structure force

With Eq. (20), the relationship between structural force and water film thickness is calculated. The calculated result shows that the structural force is small and negligible.

2.6.1.4. Calculation of water film thickness

With Eq. (13), the curve of total disjoining pressure vs. water film thickness is as shown in Fig. 10.

With Eq. (1), the capillary pressure at –2,765 m in the middle of the gas reservoir is 0.1 Mpa.

With Eq. (1), the corresponding critical pore radius is calculated to be 573 nm, and the water in the pores with a radius less than 573 nm is all bound water.

According to the iterative algorithm in Section 4, it is assumed that the initial value of the water film thickness is h = 0. With Eq. (23), the equilibrium disjoining pressure is 42,753 Pa in the pore with a radius is 611 nm. According to the relationship between the total disjoining pressure and the water film thickness, the water film thickness is about 2.1 nm.

Using the new water film thickness, recalculate a disjoining pressure, and the final water film thickness is still

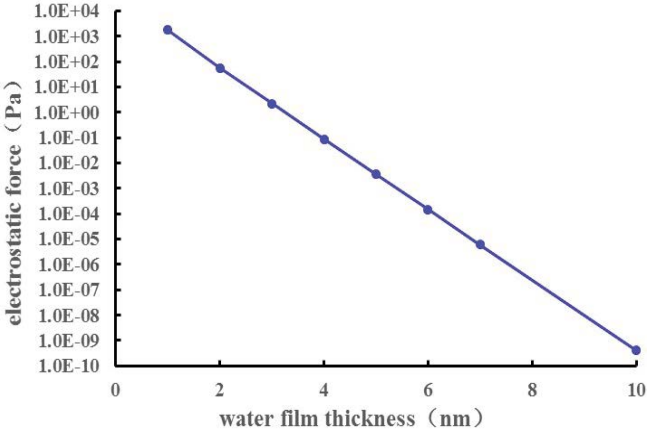

Fig. 8. Relationship between electrostatic force and water film thickness.

Table 1
Basic parameter table

Material type	Dielectric constant ε	Refractive index n
Quartz	3.8	1.448
Water	80.25	1.3333
Air	1	1

2.1 nm with graphical method. It also confirms Hall's view that the water film thickness is too small compared to pore radius, and it can be ignored directly in Eq. (6).

2.6.2. Influence of formation depth on water film thickness

At the depth of –2,755; –2,760 and –2,765 m, the gas and water pressure difference, or capillary pressure calculated by gas and water pressure gradients are 0.17, 0.14 and 0.1 MPa, respectively. The corresponding critical pore radius are 334.52, 422.48 and 573.2 nm, respectively.

As shown in Fig. 11, taking the pore radius is 611 nm as an example, according to Eq. (12), the equilibrium disjoining pressures in the pores of different depths are 114,129; 78,441 and 42,753 Pa, respectively.

The calculated water film thicknesses in the pores are 1.7, 1.8 and 2.1 nm, respectively. The results show that with the same pore radius, the water film thickness increases slightly with the increase of the altitude. However, the water film thickness under various conditions is relatively small compared to the pore radius ($r > r_c$), which is negligible.

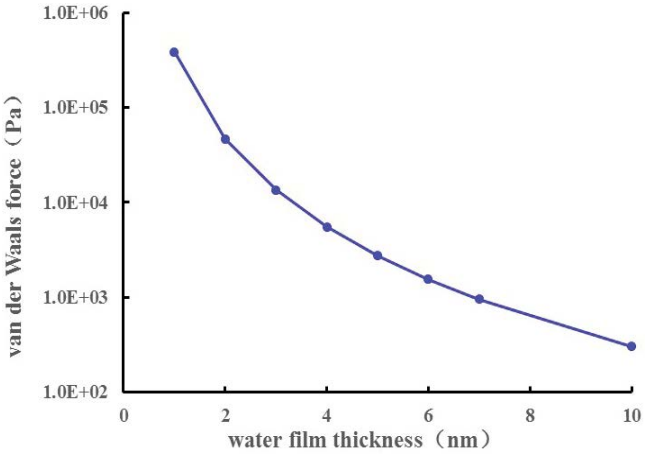

Fig. 9. Relationship between van der Waals force and water film thickness.

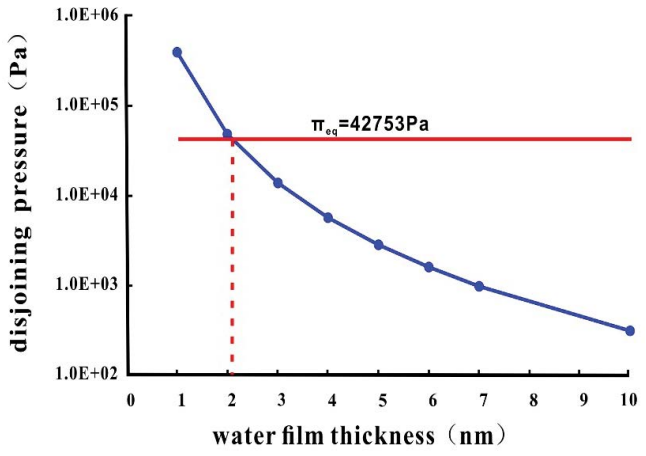

Fig. 10. Calculate water film thickness with graphical method.

2.7. Verification of water film thickness

When the disjoining pressures are 1.5 × 10^{-4} MPa and 3.0 × 10^{-4} MPa, Зорин measured the water film thicknesses of the KCl aqueous solution with 0.1 mol/m^3 on the quartz plate are 100 and 75 nm, respectively [18]. Much higher than the water film thickness that calculated in the previous section.

Since the capillary bundle model used in the previous section does not apply to quartz plates, the relevant formula should be improved. If the gas/liquid/solid interface is a flat, so the curvature radius is $R_1 = R_2 = \infty$, then Eq. (3) can be further simplified as follow:

$$p_c = p_g - p_w = \Pi_{eq} \tag{24}$$

That is:

$$\Pi_{eq} = p_c = p_g - p_w \tag{25}$$

In the water film thickness calculation method described in Section 5, the water film thickness on the quartz plate can be calculated by replacing Eq. (12) with Eq. (25).

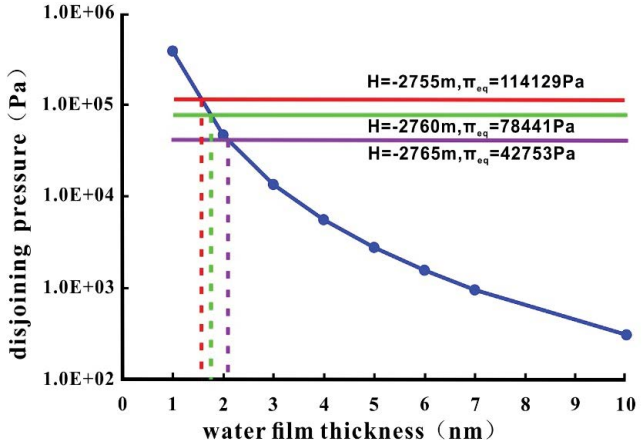

Fig. 11. Thickness of water film at the same pore radius with different depths.

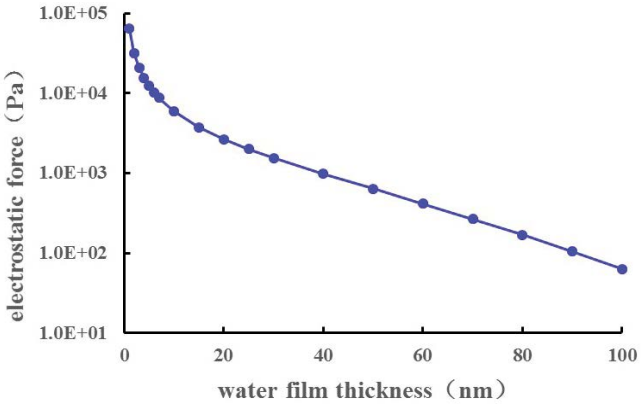

Fig. 12. Relationship between electrostatic force and water film thickness.

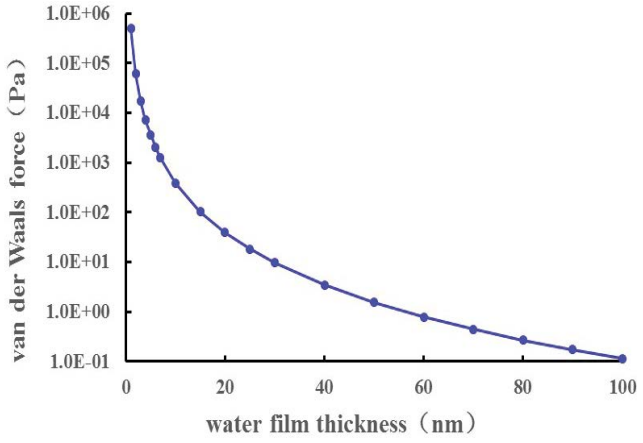

Fig. 13. Relationship between van der Waals force and water film thickness.

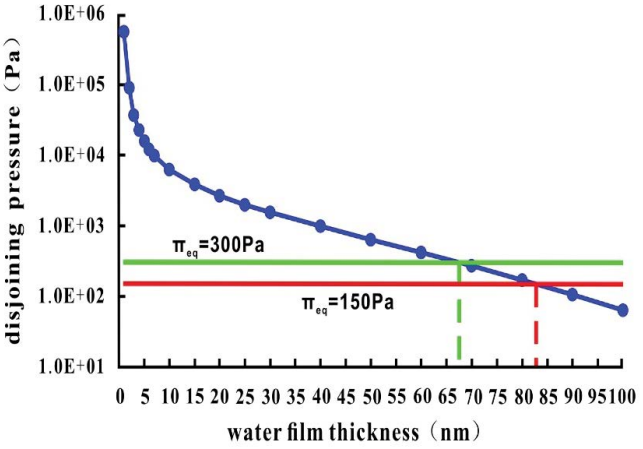

Fig. 14. Calculate water film thickness with graphical method.

Assuming the cationic valence is z = 1, and the temperature is T = 293 K. The zeta potential of quartz in aqueous solution under the condition of salinity is –110 mV [19], and the other parameters are shown in Table 1.

With Eq. (18), according to the parameters shown in Table 1, the Hamaker constant is calculated as -9.69×10^{-21} J. With Eq. (14), the calculation of the relationship between electrostatic forces $\Pi_{DLR}(h)$ and water film thickness is shown in Fig. 12. With Eq. (17), the calculation of the relationship between van der Waals forces and water film thickness is shown in Fig. 13. The structure forces calculated by Eq. (20) are very small and negligible.

Compared with Figs. 12 and 8, and Figs. 13 and 9, it can be seen that the decrease of electrostatic forces is larger than that of van der Waals forces after the increase of water salinity. All of this indicate that the electrostatic repulsion and the van der Waals force being the forces to keep the water film stable when the water salinity is low. When the salinity of the formation water is quite large in real gas reservoir, only the van der Waals force is the main force to keep the water film stable, so the water film thickness decreases with the increase of the salinity.

With Eq. (13), the relationship between total disjoining pressures and water film thickness is shown in Fig. 14. When the disjoining pressures were 1.5×10^{-4} MPa and 3.0×10^{-4} MPa, the corresponding water film thicknesses were 83 and 67 nm, respectively. The error of the water film thickness test results in the literature was 17% and 11%.

3. Conclusions

It can be seen from the DLVO theory that in the high salinity formation aqueous solution, the structure force is negligible and the electrostatic force is small. van der Waals force is the main force to keep the water film stable. When the salinity of the formation water is low, the electrostatic force and van der Waals force are the main forces to keep the water film stable.

The higher the distance from the gas/water interface, the greater the pressure difference between the gas phase and the water phase in the pores. The results of parameter sensitivity analysis show that even in the same pore radius r, the water film thickness in the higher position of the gas reservoir is smaller than that of the lower part due to the pressure difference of gas/water two-phase.

In the formation water with high salinity, the electrolyte compression double layer reducing the disjoining pressure between the interfaces of the water film, so the water film thickness in pores underground is small. According to the results of parameter sensitivity analysis, the bound water in the gas reservoir is mainly in the form of capillary water, and the water film thickness in the pores is much smaller than the pore radius, so the influence of water film thickness on the gas seepage process can be negligible, which is not so important as thought before.

Acknowledgements

The authors gratefully acknowledge the funding from the National Key Research and Development Program of China (The Chengdu University of Technology Subcontract No. 2016ZX05034002-006 and Sinopec Huabei Sub–Company Subcontract No. 2016ZX05048), which provided support for the work done here.

Conflict of interest statement

The authors declare that there is no conflict of interest regarding the publication of this paper. We declare that we do not have any commercial or associative interest that represents a conflict of interest in connection with the work submitted.

References

[1] X.P. Yang, W.Z. Zhao, C.N. Zou, M. Chen, Y. Guo, Origin of low-permeability reservoir and distribution of favorable reservoir, Acta Petrolei Sin., 28 (2007) 57–61.
[2] R.F. Wang, P.P. Shen, Z.Q. Song, H. Yang, Characteristics of micro-pore throat in ultra-low permeability sandstone reservoir, Acta Petrolei Sin., 30 (2009) 560–563.
[3] Y. Cheng, Z.P. Song, J.F. Jin, J.B. Wang, T. Wang, Experimental study on stress wave attenuation and energy dissipation of sandstone under full deformation condition, Arabian J. Geosci., 12 (2019) 1–14, doi: 10.1007/s12517-019-4915-x.

[4] B.V. Derjaguin, N.V. Churaev, Structural component of disjoining pressure, J. Colloid Interface Sci., 49 (1974) 249–255.
[5] M.L. Gee, T.W. Healy, L.R. White, Hydrophobicity effects in the condensation of water films on quartz, J. Colloid Interface Sci., 140 (1990) 450–465.
[6] N. Nishiyama, T. Yokoyama, Estimation of water film thickness in geological media associated with the occurrence of gas entrapment, Procedia Earth Planet. Sci., 7 (2013) 620–623.
[7] A.D. Ward, R. Ottewill, R.D. Hazlett, An investigation into the stability of aqueous films separating hydrocarbon drops from quartz surfaces, J. Pet. Sci. Technol., 24 (1999) 213–220.
[8] G.S. He, T. Tang, Petrophysics, Petroleum Industry Press, Beijing, 2011.
[9] A.C. Hall, S.H. Collins, J.C. Melrose, Stability of aqueous wetting films in Athabasca Tar Sands, Soc. Petrol. Eng. J., 23 (1982) 249–258.
[10] J. Gregory, Interaction of unequal double layers at constant charge, J. Colloid Interface Sci., 51 (1975) 44–51.
[11] T.K. Tokunaga, Correction to DLVO-based estimates of adsorbed water film thicknesses in geologic CO_2 reservoirs, Langmuir, 29 (2013) 3152, doi: 10.1021/la400463a.
[12] B. Chandrasekhar, D.N. Rao, Application of DLVO theory to characterize spreading in crude oil-brine-rock systems, Arzneimittel-Forschung, 21 (2004) 474–476.
[13] G.J. Hirasaki, Wettability: fundamentals and surface forces, SPE Form. Eval., 6 (1991) 217–226.
[14] R. Sutton, An Improved Model for Water-Hydrocarbon Surface Tension at Reservoir Conditions, Paper Presented at the SPE Annual Technical Conference and Exhibition, New Orleans, Louisiana, October 2009.
[15] H.H. Uhlig, F.G. Keyes, The dependence of the dielectric constants of gases on temperature and density, J. Chem. Phys., 1 (1933) 155–159.
[16] H.J. Achtermann, J. Hong, W. Wagner, A. Pruss, Refractive index and density isotherms for methane from 273 to 373 K and at pressures up to 34 MPa, J. Chem. Eng. Data, 37 (1992) 414–418.
[17] J.N. Israelachvili, Chapter 13 – Van der Waals Forces between Particles and Surfaces, In: Intermolecular and Surface Forces, Academic Press, 2011, pp. 253–289.
[18] Зорин, З.М. и др.: Смачивающие пленки водных растворов электролитов на поверхности плавленного кварца, Коллоидю Журн, 52 (1990) 666–673.
[19] C.L.A. Berli, M.V. Piaggio, J.A. Deiber, Modeling the zeta potential of silica capillaries in relation to the background electrolyte composition, Special Issue: Solvent Effects in Capillary Electrophoresis, 24 (2003) 1587–1595.